Euler and Navier-Stokes Leeside Flows over Supersonic Delta Wings

S. N. McMillin* and J. L. Thomas†
NASA Langley Research Center, Hampton, Virginia
and
E. M. Murman‡
Massachusetts Institute of Technology, Cambridge, Massachusetts

Numerical simulations of several distinctly different types of leeside flowfields over higly swept, sharp, leading-edge delta wings in supersonic flow were obtained using Euler and Navier-Stokes solvers. The Euler code was seen to be adequate for predicting primary flow structures (leading-edge vortex and crossflow shock), whereas the Navier-Stokes code was capable of predicting primary and secondary flow structures (i.e., secondary vortex and shock-induced separation). A comparison of laminar and turbulent Navier-Stokes solutions for leading-edge separated flows for which the boundary-layer state was known indicated that the turbulent boundary-layer model is more accurate in predicting the effect of the boundary layer on the flowfield. Also, for several cases, the Navier-Stokes code indicated detailed flow structures not observed in the qualitative experimental data available.

Introduction

THE development and experimental validation of advanced aerodynamic computational techniques such as Euler and Navier-Stokes codes will eventually provide aerodynamic design capability heretofore not possible. In the past, aerodynamic design methodology for low supersonic Mach numbers has been limited to a relatively simple flow model. For example, in the 1960's and 1970's, wing designs[1] for SST or fighter applications were based on solutions to the linearized potential equation and were therefore limited to subsonic crossflows. More recent high-lift wing designs[2] have employed methodology based on solutions of the nonlinear full-potential equations, which can treat mixed subsonic/supersonic crossflows and which model shocks. These designs are still restricted to attached flows, because of the irrotational, inviscid assumptions of full-potential theory. Vortex flap-wing designs[3] assume the existence of leading-edge vortices and have employed a methodology based on a combination of linearized potential theory and empirical data. The aerodynamicist prefers not to be limited to a particular type of flow and likes to make optimum use of both attached and separated flows. In order to achieve this, the design methodologies and procedures must be based on rather unrestricted aerodynamic computational techniques. Recently reported results[4-11] indicate that algorithms capable of solving the Euler and Navier-Stokes equations are sufficiently developed and that computer processing speeds have decreased enough to begin the necessary validation process that leads to incorporating Euler and Navier-Stokes methods into the wing design process.

Several researchers have experimentally investigated and classified the leeside flow over highly swept wings in supersonic flow. Stanbrook and Squire[12] classified separated and attached leeside flow regimes using the similarity parameters Mach number M_N and angle of attack α_N normal to the leading edge. This work has been extended further by Whitehead et al.,[13] Szodruch and Ganzer,[14] and Miller and Wood.[15] The definition of leeside flows based on the wind-tunnel experiment reported in Ref. 15 is presented in Fig. 1. The central vertical boundary of Fig. 1 is similar to the classical Stanbrook and Squire boundary between separated and attached flow. The flow types to the left of this boundary are as follows, starting at the bottom of the figure: leading-edge separation bubble with no shock, primary and secondary vortex with no shock, and primary and secondary vortex with shock. The flow types to the right of the Stanbrook and Squire boundary, in the same order, are as follows: shock with no separation, shock-induced separation, and separation bubble with shock.

The purpose of this paper is to present Euler and Navier-Stokes results for a case from each of the six flow regimes that have been observed experimentally on the leeside of flat, sharp, leading-edge delta wings at supersonic speeds. The computed results will be compared with one another and with experimental data previously reported in Ref. 15. There will also be a discussion of the effect of the boundary-layer state in the Navier-Stokes solutions for the flow conditions examined in this paper.

Experimental Setup and Models

Figure 1 shows the flow regimes that are examined in this paper and the experimental data points used to define the regimes. The data were obtained in a wind-tunnel experiment[15] conducted in the NASA Langley Unitary Plan Wind Tunnel (UPWT) on four delta-wing models that varied in leading-edge sweep ($\Lambda = 75$, 67.5, 60, and 52.5 deg). Each model had a total span of 1 ft and a thickness of 0.3 in. at the trailing edge. The upper surface of each model was flat, and the leading edge was made sharp (10-deg angle normal to the leading edge located on the lower surface). Each model was in-

---

Presented as Paper 87-2270 at the AIAA 5th Applied Aerodynamics Conference, Monterey, CA, Aug. 17-19, 1987; received Feb. 29, 1988; revision received Nov. 15, 1988.

*Aero-Space Technologist, Supersonic/Hypersonic Aerodynamics Branch, High-Speed Aerodynamics Division. Member AIAA.

†Aero-Space Technologist, Analytical Methods Branch, Low-Speed Aerodynamics Division. Associate Fellow AIAA.

‡Professor. Fellow AIAA.

strumented with a row of pressure orifices located 1 in. forward of the trailing edge. Transition strips of grit were sprinkled on the upper surface 0.2 in. behind the model leading edge to insure turbulent boundary-layer flow over the model at attached-flow conditions. The four models were each tested at $M = 1.7$, 2.0, 2.4, and 2.8 over an angle-of-attack range of 0–20 deg and at a Reynolds number of 2.0×10^6/ft. In addition to the surface pressure data obtained near the trailing edge, vapor-screen photographs were also obtained. The vapor-screen flow-visualization technique provides qualitative data on the flowfield and was the primary source of information used in defining the flow regimes of Fig. 1. However, the sensitivity of the technique is not known at this time.

Computational Algorithms

Because the experimental data have shown the leeside flow to develop conically and the leeside surface geometry of a flat delta wing is obviously conical, it was decided that conical solutions would adequately represent the flows being investigated in this study. The assumption of conical flows significantly reduced the required computational resources and made possible the examination of all significant cases. The Euler code of Ref. 5 and the Navier-Stokes code of Ref. 4 were selected for this study because each code has previously been used to predict delta wing leeside flows for a few selected cases.

The computational method utilized in the Euler code has been discussed in detail in several references (5, 16, and 17), and only a brief summary will be given here. The full three-dimensional unsteady Euler equations are transformed to a conical coordinate system. A Jameson type of finite-volume method is used to discretize the equations in conservative form, and a Runge-Kutta method is used to integrate the pseudo-unsteady equations to achieve steady-state solutions. Boundary conditions enforce tangential flow at the body surface and freestream conditions on the outer boundary, which is outside the bow shock.

The Euler equations themselves contain no dissipation, and the centered spatial differences are not dissipative to lowest order. Artificial damping or viscosity is required to damp out high-frequency modes of the discrete equations and to capture shocks. Blended fourth- and second-difference dissipation terms are added to the discretized inviscid equations for these two purposes, respectively.

For a sharp-edge geometry like that which is considered here, a Kutta condition provides the mechanism for locating the point at which the flow separates from the wing to form a primary vortex. In the calculations, the Kutta condition is enforced implicitly by the artificial damping. Because the separation point is determined by the geometry, its position is insensitive to the magnitude of both physical and numerical viscosity for Reynolds numbers of interest. The artificial viscosity also provides a mechanism for creating losses. Computations and analysis have shown that the levels of these losses are not sensitive to the levels of damping.[16,18]

The computational method utilized in the Navier-Stokes code has been discussed in detail in Refs. 4 and 19–23; only a brief summary will be given here. The thin-layer approximation to the three-dimensional, time-dependent, compressible Navier-Stokes equations are transformed to a generalized coordinate system. The convective and pressure terms are differenced with the upwind-biased flux-difference splitting approach of Roe,[20] whereas the shear stress and heat-transfer terms are centrally differenced. For all the results presented, a third-order discretization of the convective and pressure terms is used. Because the shear stress and heat-transfer terms are differenced with second-order accuracy, the global accuracy is second order. The spatial differencing scheme is very similar to that in Ref. 4, except that flux-difference rather than flux-vector splitting is used for the convective and pressure terms. The flux-difference splitting approach includes information about all differencing waves by which adjacent cells interact and is demonstrated in Ref. 22 to be more accurate than the flux-vector splitting approach in the boundary-layer region.

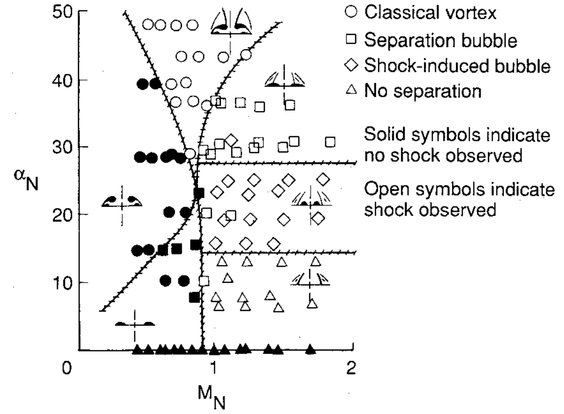

Fig. 1 Classification of experimental data for sharp-edged delta wings.[15]

The time-differencing algorithm used in the Navier-Stokes code is a spatially split approximate-factorization method. It is difficult to linearize exactly the residual terms arising with Roe's flux-difference splitting approach, and an approximate linearization is used. The resulting implicit discretization is conservative in time and is, in practice, similar to that used in Ref. 23, corresponding to a first-order flux-vector splitting linearization in time.

The turbulent boundary-layer calculations are made with an algebraic two-layer eddy-viscosity model. The model includes the modifications incorporated by Degani and Schiff[24] necessary to insure that in vortical flows the viscous length scales are determined by the boundary layer on the body or wing. The model was recently used by Newsome and Adams[25] in the accurate prediction of elliptical missile body flows at large angles of attack and yaw.

For the conical flow solutions obtained by the Navier-Stokes code, a single array of crossflow volumes is constructed such that the inflow and outflow planes are scaled by a conical transformation. At each iteration, the inflow conditions are updated with the results of the previous iteration until convergence occurs. The solutions in all cases were impulsively started from freestream initial conditions. Boundary conditions consisted of freestream conditions on the outer boundary, reflection conditions in the crossflow symmetry plane, and no-slip adiabatic wall or specific wall temperature conditions on the body surface.

Results and Discussion

A systematic approach was taken in selecting cases from Fig. 1 for the purpose of the study. For all cases, the Mach number was held constant at 2.8 with leading-edge sweep and/or angle of attack varying. In Fig. 2, the selected cases are seen to cover completely all six of the flow regimes. In the interest of space, only one case from each flow regime will be presented here. The six cases to be presented are numbered in Fig. 2. The vapor-screen photographs corresponding to each case are presented as Fig. 3. Note the location of the bow shock for cases 4–6.

The cross-sectional geometry at the trailing edge of the configuration is used for all of the conical solutions. The conical self-similarity assumption implies that this section is extended conically forward to a point and aft to infinity. In all of the plots, the y and z coordinates are normalized by the value of y at the leading edge of the wing.

Computational Solutions

Each of the grids used in obtaining the Euler solutions consisted of 128 radial and 128 circumferential (128×128) points.

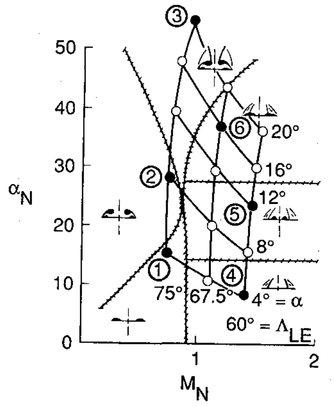

Fig. 2 Test matrix for numerical study; Mach number held constant at 2.8.

Case 1: Λ = 75 deg, α = 4 deg **Case 4: Λ = 60 deg, α = 4 deg**

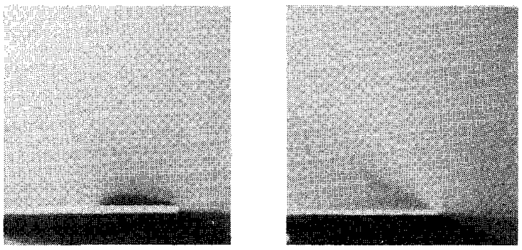

Case 2: Λ = 75 deg, α = 8 deg **Case 5: Λ = 60 deg, α = 12 deg**

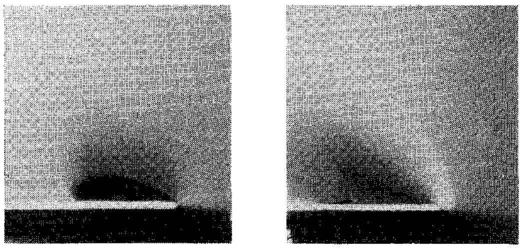

Case 3: Λ = 75 deg, α = 20 deg **Case 6: Λ = 67.5 deg, α = 16 deg**

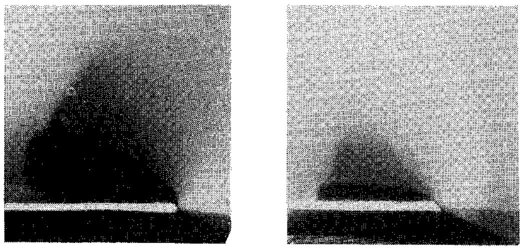

Fig. 3 Vapor-screen photographs of six cases; $M = 2.8$.

The Euler grid was generated using a code developed at MIT based on the method of Ref. 26, with modifications to enforce conditions on grid aspect ratio rather than normal spacing at the body and outer boundaries. For each case, calculations were first obtained on coarser grids and then interpolated for use as initial conditions on the 128 × 128 grids. The solutions were run for 500 iterations on this grid. All six of the cases except case 6 ($\Lambda = 67.5$ deg, $\alpha = 16$ deg, $M = 2.8$) converged to an acceptable steady-state solution. The general features and force coefficients for case 6 appeared satisfactory, but the residual did not reach a steady-state level. The flow pattern associated with this case is apparently very sensitive with the Euler equation model.

The grids used with the Navier-Stokes code were generated numerically using the code of Ref. 27, which is based on the method of Ref. 26. Each grid consisted of 75 radial and 151 circumferential (75 × 151) points. The radial grid point stretching distribution was exponential at the body, with a smooth transition to a milder geometric stretching in the outer part of the grid.

In Ref. 28, it was determined that the type of grid spacing through the boundary layer could have a significant impact on the results. For example, for a turbulent boundary-layer condition, a stretched grid in the boundary layer (which clustered points near the surface) yielded more accurate results than a uniform grid. The opposite trend was found to exist for a laminar boundary-layer condition. Hence, for the purposes of this study, the grid for the turbulent boundary-layer cases is more stretched than that of the laminar boundary-layer cases. The turbulent spacing grid for each geometry had a minimum spacing of $\Delta s/x_{TE} = 0.3 \times 10^{-4}$ at the wall, where x_{TE} is the steamwise location of the trailing edge. This minimum spacing was based on the criterion of having 1–2 points in the viscous sublayer. The laminar spacing grid had $\Delta s/x_{TE}$ of 0.5×10^{-4} for the 75-deg delta wing and $\Delta s/x_{TE}$ of 0.1×10^{-4} for the 67.5 and 60 deg delta wings. These values were based on the criterion of having 15–20 points in the boundary layer. Also to be noted here is the fact that the leading edge was rounded with a leading-edge radius of $r/x_{TE} = 0.2 \times 10^{-3}$. This modification to the geometry allowed a smoother grid about the leading edge to be achieved for use in the Navier-Stokes code. The span of the modified cross section was 99.9% of that of the original span.

The laminar boundary-layer solutions were obtained for cases 1–3 and 6. For case 1 ($\Lambda = 75$ deg, $\alpha = 4$ deg, $M = 2.8$), it was not possible to obtain a converged laminar solution on the laminar grid. Consequently, this case was repeated on the turbulent grid, and a converged laminar solution was obtained. The reason for this is unknown at the present time. Turbulent boundary-layer solutions were also obtained for all six cases using the turbulent spacing grid.

A typical problem in obtaining the Navier-Stokes solutions was that the residual entered into a limit-cycle oscillation although flowfield quantities such as lift coefficient and total pressure had reached an acceptable convergence. This characteristic has been associated with the limiter used in the differencing scheme. Solutions were also obtained with the flux-vector splitting algorithm, with only small differences noted from the results shown, indicating that the truncation error levels are small.

Computational Results and Comparisons

The Euler and turbulent Navier-Stokes solutions for all six cases are presented later. As discussed in Ref. 15, the models had grit located 0.2 in. behind the leading edge to insure fully turbulent boundary-layer flow over the model at attached leading-edge flow conditions. However, a question arises as to the boundary-layer condition for the flow separating at the leading edge, reattaching near the centerline, and flowing outward on the wing under a primary vortex. Thus, laminar Navier-Stokes solutions are presented for the separated flow cases (i.e., cases 1–3 and 6). However, the Reynolds numbers (2.0×10^6/ft) are sufficiently high to expect the flow to be turbulent at the trailing edge via natural transition,[29] based on subsonic data indicating that transition will occur at a Reynolds number of approximately 0.9×10^6. The computed surface-pressure distributions are summarized and compared with experiment in Fig. 4. Following is a discussion on each of the six cases, along with other supporting data presentations. Portions of the data are presented in the form of total pressure contours, which define vortical structures as they appear in vapor-screen photographs. Likewise, crossflow Mach number contours are used in some of the data presentation because these contours define shock systems as they appear in vapor-screen photographs.

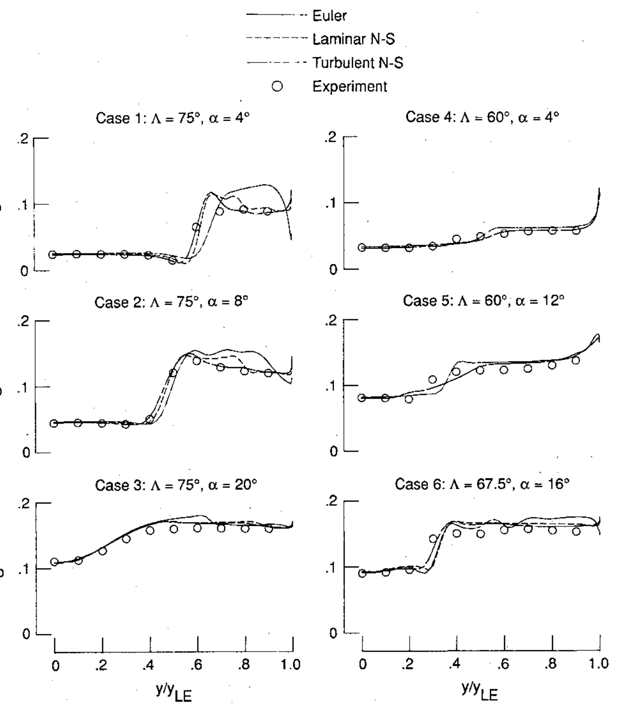

Fig. 4 Comparison of computational and experimental surface-pressure distributions for six cases, $M = 2.8$.

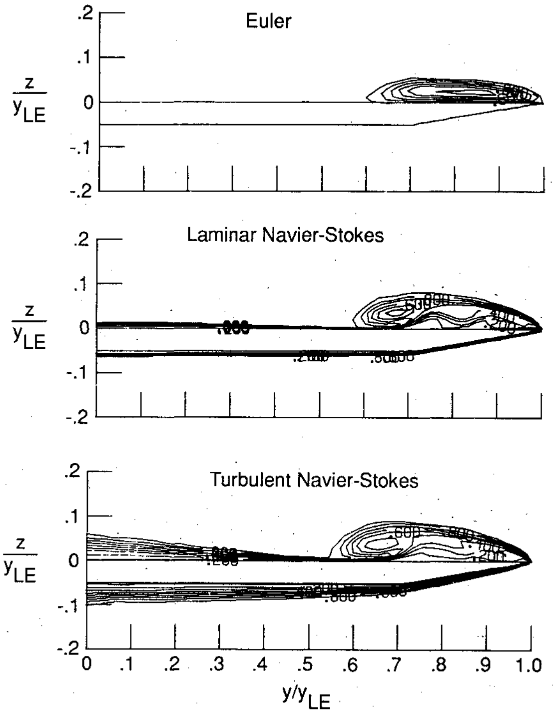

Fig. 5 Total pressure contours from the Euler, laminar Navier-Stokes, and turbulent Navier-Stokes solutions for case 1; $\Lambda = 75$ deg, $\alpha = 4$ deg, and $M = 2.8$.

Total pressure contour plots from the Euler, laminar Navier-Stokes, and turbulent Navier-Stokes solutions for case 1 ($\Lambda = 75$ deg, $\alpha = 4$ deg, $M = 2.8$) are presented in Fig. 5. The vapor-screen photograph (Fig. 3) has been interpreted as a separation bubble in Ref. 15. A separation bubble is defined as having its entire rotational flow contained within its boundaries, and it exhibits no secondary separation. All three solutions have a primary vortex separating at the leading edge, with the core lying close to the surface of the wing such that the reattachment line coincides with the termination of the vortex. In this respect, each solution agrees with Miller and Wood's interpretation[15] of the vapor-screen photograph. However, the Navier-Stokes solutions are both seen to have at least one secondary vortex beneath the primary vortex that does not agree with the vapor-screen interpretation from Ref. 15. The vapor-screen flow visualization technique may not be sensitive enough to detect the separate flow structures seen in the contour data (Fig. 5) since the primary vortex lies so close to the wing or the numerical solution may be in error. In examining the surface-pressure distributions (Fig. 4), the turbulent solution agrees more closely with the experimental data, whereas the Euler solution substantially overpredicts the expansion due to the primary vortex. The laminar and turbulent Navier-Stokes surface-pressure distributions agree closely, except in the region under the primary vortex where the laminar solution exhibits two secondary vortices. The flow beneath the primary vortex in the turbulent solution is more resistant to separation, and the one secondary vortex that forms is weaker than the two secondary vortex structures predicted in the laminar solution.

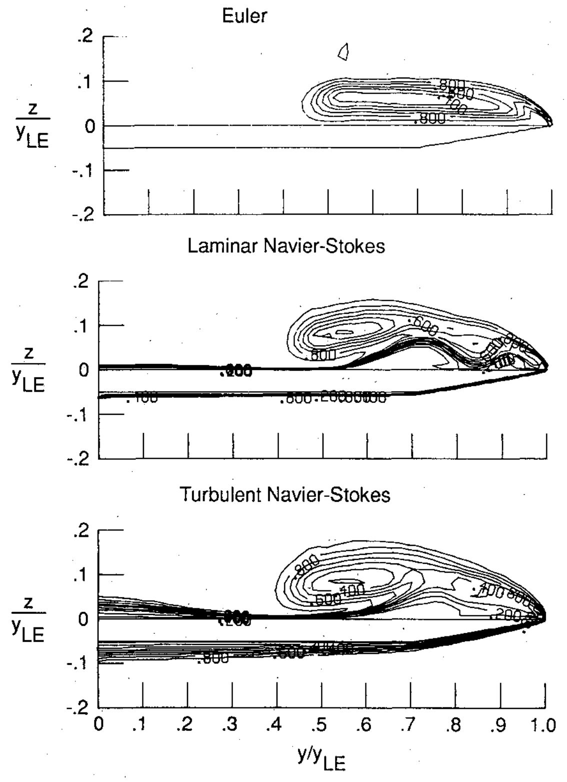

Fig. 6 Total pressure contours from the Euler, laminar Navier-Stokes, and turbulent Navier-Stokes solutions of case 2; $\Lambda = 75$ deg, $\alpha = 8$ deg, and $M = 2.8$.

Figure 6 shows the total pressure contour plots for each of the Euler, laminar Navier-Stokes, and turbulent Navier-Stokes solutions for case 2 ($\Lambda = 75$ deg, $\alpha = 8$ deg, $M = 2.8$). Reference 15 interprets the flow structure evident in the vapor-screen photograph to be that of a primary vortex with a secondary vortex. The contour data of Fig. 7 show that the Euler and Navier-Stokes codes (regardless of boundary-layer condition) predict the formation of a vortex from the leading edge. The Euler code does not predict the secondary vortex since this structure results from a separtion in the boundary layer. However, the laminar Navier-Stokes code predicts not only this secondary vortex but also a second secondary vortex (rotation in the same sense as the first secondary vortex), which is not evident in the vapor-screen photograph. Consistent with the observations made for case 1, the secondary vortex of the turbulent solution appears weaker than the more inboard second-

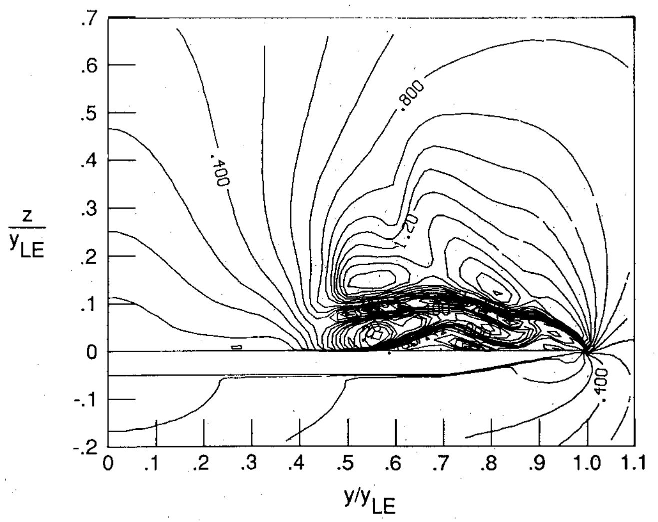

Fig. 7 Crossflow Mach number contours from the laminar Navier-Stokes solutions of case 2; $\Lambda = 75$ deg, $\alpha = 8$ deg, and $M = 2.8$.

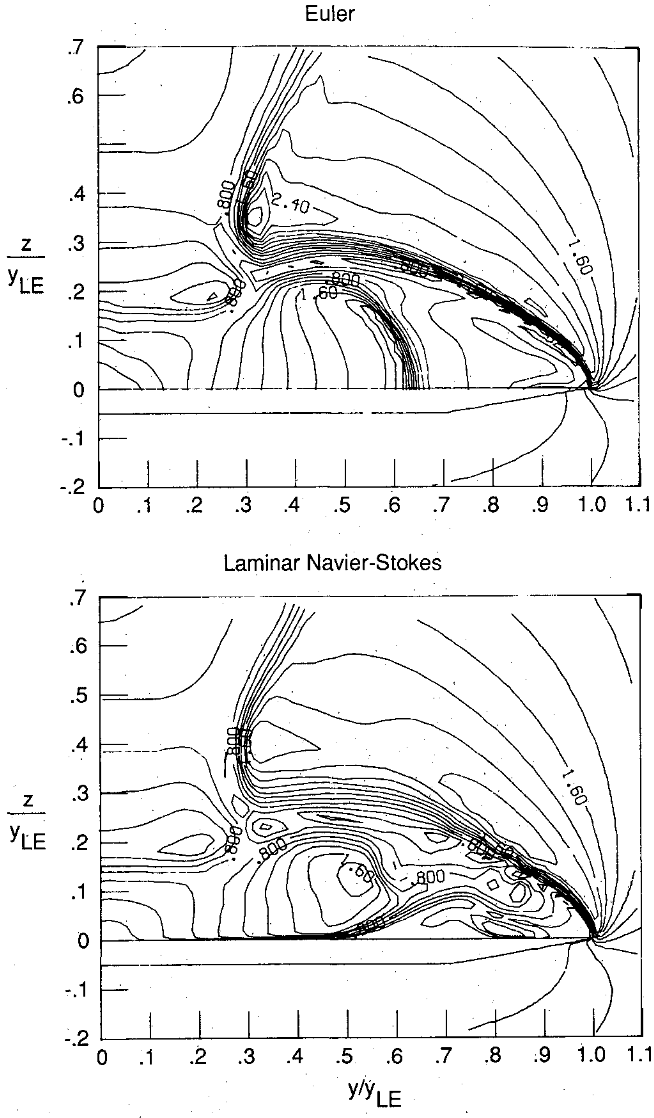

Fig. 8 Crossflow Mach number contours from the Euler and laminar Navier-Stokes solutions of case 3; $\Lambda = 75$ deg, $\alpha = 20$ deg, and $M = 2.8$.

ary vortex predicted in the laminar solution. Thus, the turbulent solutions is in better agreement with both the vapor-screen photograph and the surface-pressure data.

The crossflow Mach number contour plot from the laminar Navier-Stokes solution for case 2 is shown in Fig. 7. The crossflow shock atop the primary vortex evident in the figure is typical of each of the three solutions. The interpretation from Ref. 15 for this case does not mention any crossflow shock system. However, the changing gray levels atop the primary vortex in the vapor-screen photograph correspond very well to the computed crossflow shock structure (Fig. 7). The crossflow shock is weak, with a total pressure loss less than 10% and is not evident in the total pressure contour data since the total pressure loss is less than the increment used in contouring the total pressure data. Thus, the crossflow Mach number contours more closely resemble the crossflow shock structures as seen in the vapor-screen photographs, whereas the total pressure contours more closely resemble the vortical structures in the vapor-screen photographs.

Figure 8 shows the crossflow Mach number contour plots from the Euler and laminar Navier-Stokes solutions for case 3 ($\Lambda = 75$ deg, $\alpha = 20$ deg, $M = 2.8$). The contour data of Fig. 8 show that both codes predict a vortex separating at the leading edge, with a shock forming on top of the primary vortex. A crossflow shock is also seen to form between the primary vortex and its counterpart across the longitudinal plane of symmetry. These flow structures are seen very clearly in the corresponding vapor-screen photograph of Fig. 3. The vapor-screen photograph also shows a secondary vortex forming beneath the primary vortex. The Euler code predicts a shock rather than a secondary vortex in this region. This shock is evident in the Euler surface-pressure distribution (Fig. 4). In contrast, the laminar Navier-Stokes contour data show the formation not only of the secondary vortex but also of a shock between the primary and secondary vortices, which is not evident in the vapor-screen photograph. The turbulent Navier-Stokes solution, which is not presented in Fig. 8, is very similar to the laminar solution, except that the secondary vortex is weaker than that of the laminar solution. This observation is also reflected in the surface-pressure data (Fig. 4). In the region of the secondary vortex, the turbulent solution has a more level pressure distribution and is in better agreement with the experimental data.

As stated before, the vapor-screen photograph does not show a crossflow shock occurring between the primary and secondary vortices of this case. This structure is clearly evident in the crossflow Mach number contour data of both Navier-Stokes solutions and in the total pressure contour data (not presented). These data also show the crossflow shock above the primary vortex core. Thus, the flow visualization technique of vapor screens is apparently not sensitive enough to detect such a detailed flow structure, assuming that the Navier-Stokes solutions are correct.

The contour data for case 4 ($\Lambda = 60$ deg, $\alpha = 4$ deg, $M = 2.8$), omitted here for brevity, appear very similar to the corresponding vapor-screen photograph (Fig. 3). The flow structure is that of attached flow with a crossflow shock occurring inboard of the leading edge. In examining the surface-pressure data (Fig. 4), the Euler and turbulent Navier-Stokes codes predict approximately the same location for the crossflow shock ($y/y_{\mathrm{LE}} = 0.5$). The Euler code predicts a slightly stronger shock.

The crossflow Mach number contour data for the Euler and turbulent Navier-Stokes solutions for case 5 ($\Lambda = 60$ deg, $\alpha = 12$ deg, $M = 2.8$) are shown in Fig. 9. The vapor-screen photograph (Fig. 3) shows that the flow is attached at the leading edge, with a shock forming inboard. According to the interpretation of Ref. 15, a shock-induced separation bubble is located below and immediately inboard of this crossflow shock. The contour data of Fig. 9 show that both codes predict attached flow at the leading edge. The Euler data show a crossflow shock occurring at $y/y_{\mathrm{LE}} = 0.35$, with no separation

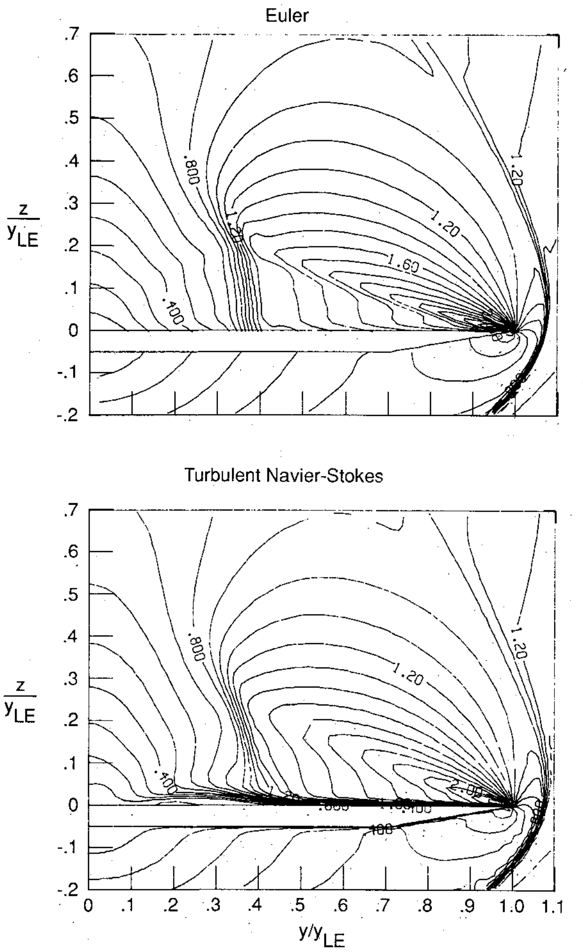

Fig. 9 Crossflow Mach number contours from the Euler and turbulent Navier-Stokes solutions of case 5; $\Lambda = 60$ deg, $\alpha = 12$ deg, and $M = 2.8$.

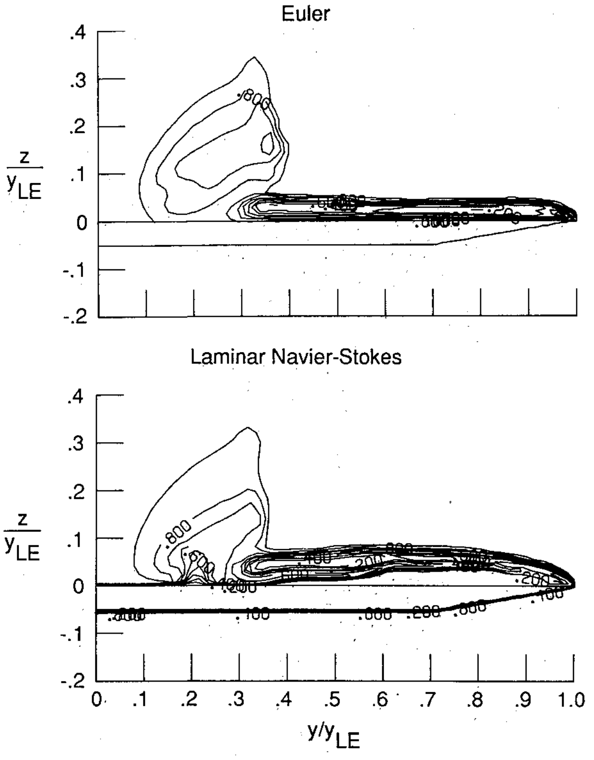

Fig. 10 Total pressure contours from the Euler and laminar Navier-Stokes solutions of case 6; $\Lambda = 67.5$ deg, $\alpha = 16$ deg, and $M, = 2.8$.

bubble evident. The turbulent Navier-Stokes data show a shock-induced separation just inboard of the crossflow shock at $y/y_{\rm LE} = 0.4$. Thus, the turbulent Navier-Stokes solution is in better agreement with the corresponding vapor-screen photograph. The different flow structures of the Euler and turbulent Navier-Stokes solutions are reflected in the surface-pressure distributions (Fig. 4). The presence of the crossflow shock is clearly seen in the Euler distribution. However, the shock-induced separation dampens the effect of the crossflow shock on the surface-pressure distribution in the turbulent Navier-Stokes solution. The turbulent Navier-Stokes distribution is in better agreement with the experimental distribution.

Figure 10 shows the total pressure contour plots for the Euler and laminar Navier-Stokes solutions for case 6 ($\Lambda = 67.5$ deg, $\alpha = 16$ deg, $M = 2.8$). The interpretation of the vapor-screen photograph for this case (Fig. 3), as found in Ref. 15, is that of a leading-edge separation bubble with a crossflow shock located atop the bubble. The contour data of Fig. 10 for both solutions agree well with the vapor-screen photograph. However, the contour data of Fig. 10, corroborated by crossflow velocity vectors, indicate that both codes predict a structure resembling a vortex separating at the leading edge, with the core of the vortex lying close to the surface of the wing. As can be seen in the total pressure data of Fig. 10 and the velocity vectors (not presented here), the laminar Navier-Stokes code predicts a secondary vortex occurring beneath the primary vortex, which is not seen in the vapor-screen photograph. From the same data, it can be seen that the laminar Navier-Stokes code predicts the formation of a shock-induced vortex occurring just inboard of the shock/vortex system. The Euler code also predicted the formation of this shock-induced vortex. This shock-induced vortex appears to be a weak flow structure and is not evident in the vapor-screen photograph. The turbulent Navier-Stokes solution for this case is very similar to the laminar solution, except that the secondary vortex and the shock-induced vortex are weaker. These differences between the laminar and turbulent Navier-Stokes solutions are evident in the surface-pressure distributions (Fig. 4). The turbulent Navier-Stokes surface-pressure distribution is seen to be in better agreement with the experimental data.

Conclusions

The leeside flowfields over higly swept, sharp, leading-edge delta wings in supersonic flow were numerically simulated using Euler and Navier-Stokes solvers. Distinctly different types of flowfields have been found through experimental investigations. Computations for six cases were shown, each corresponding to a different flow type. The Euler code was seen to be adequate for predicting the formation of the primary vortex and embedded crossflow shock flow structures and generally overestimated the expansion due to the vortex. The Navier-Stokes code, in modeling the effects of viscosity, was capable of predicting secondary flow structures observed experimentally (such as the secondary vortex under a primary vortex and shock-induced separation). The Navier-Stokes solutions also indicated that a separation bubble, as defined in the experimental investigation, is merely a shallow primary vortex whose core lies close to the surface of the wing. However, the Navier-Stokes code indicated detailed flow structures not observed in the qualitative experimental data (i.e., vapor-screen photographs). A comparison of laminar and turbulent Navier-Stokes solutions for leading-edge separated flows for which the boundary-layer state was not known indicated that the turbulent solutions agreed more closely with the experimental data. It was observed that because the turbulent boundary-layer model is more resistant to separation, the secondary structures resulting from crossflow boundary-layer separation were weakened. Quantitative flowfield data are needed to resolve the differences between the computed and experimentally observed flow structures.

Acknowledgments

The portion of the research performed at MIT was supported by the Office of Naval Research under Grant N00014-86-K-0288. The authors would like to acknowledge the contributions of Kenneth G. Powell.

References

[1] Brown, C., McLean, F., and Klunker, E., "Theoretical and Experimental Studies of Cambered and Twisted Wings Optimized for Flight at Supersonic Speeds," *Proceedings of the 2nd International Congress of Aeronautical Sciences, Advances in Aeronautical Science*, Vol. 3, edited by T. Von Karman et al., Pergamon, Oxford, 1962, pp. 415–431.

[2] Pittman, J. I., Miller, D. S., Mason, W. H., "Supersonic, Nonlinear, Attached-Flow Wing Design for High Lift with Experimental Validation," NASA TP-2336, Aug. 1984.

[3] Lan, C. E. and Chang, J. F., "VORCAM—A Computer Program for Calculating Vortex Lift Effect of Cambered Wings by the Suction Analogy," NASA CR-165800, Nov. 1981.

[4] Thomas, J. L. and Newsome, R. W., "Navier-Stokes Computations of Lee-Side Flow over Delta Wings," AIAA Paper 86-1049, May 1986.

[5] Murman, E. M., Powell, K. G., Miller, D. S., and Wood, R. M., "Comparison of Computations and Experimental Data for Leading-Edge Vortices—Effects of Yaw and Vortex Flaps," AIAA Paper 86-0439, Jan. 1986.

[6] Arlinger, B. G., "Computation of Supersonic Flow Including Leading-Edge Vortex Flows Using Marching Euler Technique," *Proceedings of the International Symposium on Computational Fluid Dynamics*, K. Oshimi (ed.), Vol. 2, Tokyo, Japan, Sept. 1985. pp. 1–16.

[7] Murman, E. M., Rizzi, A., and Powell, K. G., "High Resolution Solutions of the Euler Equations for Vortex Flows," *Progress and Supercomputing in Computational Fluid Dynamics*, Birkhäuser, Boston, 1985, pp. 93–113.

[8] Rizzi, A. and Ericksson, L. E., "Computation of Iniviscid Incompressible Flow with Rotation," *Journal of Fluid Mechanics*, Vol. 153, April 1985, pp. 275–312.

[9] Buter, T. A. and Rizetta, D. P., "Steady Supersonic Navier-Stokes Solutions of a 75 Degree Delta Wing at Angle of Attack, *Proceedings of NASA Langley Vortex Flow Aerodynamics Conference*, NASA CP 2416, Hampton, VA, Oct. 1985, pp. 331–339.

[10] Fujii, K. and Kutler, P., "Numerical Simulation of the Viscous Flow Fields over Three-Dimensional Complicated Geometries," AIAA Paper 84-1550, June 1984.

[11] Rizetta, D. P. and Shang, J. S., "Numerical Simulation of Leading-Edge Vortex Flows," AIAA Paper 84-1544, June 1984

[12] Stanbrook, A. and Squire, L. C., "Possible Types of Flow at Swept Leading Edges," *Aeronautical Quarterly*, Vol. XV, Feb. 1964, pp. 72–82.

[13] Whitehead, A. H., Hefner, J. N., and Rao, D. M., "Lee-Surface Vortex Effects over Configurations in Hypersonic Flow," AIAA Paper 72-77, Jan. 1972.

[14] Szodruch, J. and Ganzer, U., "On the Lee-Side Flow over Delta Wings at High Angle of Attack," AGARD 247, Sept. 1978.

[15] Miller, D. S. and Wood, R. M., "Lee-Side Flow over Delta Wings at Supersonic Speeds," NASA TP-2430, June 1985.

[16] Powell, K. G., Murman, E. M., Perez, E. S., and Baron, J. R., "Total Pressure Losses in Vortical Solutions of the Conical Euler Equations," *AIAA Journal*, Vol. 25, March 1987, pp. 360–368.

[17] Powell, K. G., Murman, E. M., Wood, R. M., and Miller, D. S., "A Comparison of Experimental and Numerical Results for Delta Wings with Vortex Flaps," AIAA Paper 86-1840, June 1986.

[18] Powell, K. G., "Vortical Solutions of the Conical Euler Equations," Ph.D. Thesis, Department of Aeronautics and Astronautics, MIT, Cambridge, MA, June 1987.

[19] Vatsa, V. N., Thomas, J. L., and Wedan, B., "Navier-Stokes Computations of Prolate Spheroids at Angle of Attack," AIAA Paper 87-2627, Aug. 1987.

[20] Roe, P. L., "Characteristics Based Schemes for the Euler Equations," *Annual Review of Fluid Mechanics*, Annual Reviews, Inc., Palo Alto, CA, 1986, pp. 337–365.

[21] Anderson, W. K., Thomas, J. L., and Van Leer, B., "Comparison of Finite Volume Flux Splitting Methods for the Euler Equations," *AIAA Journal*. Vol. 24, Sept. 1986, pp. 1453–1460.

[22] Van Leer, B., Thomas, J. L., Roe, P. L., and Newsome, R. W., "A Comparison of Numerical Flux Formulas for the Euler and Navier-Stokes Equations," AIAA Paper 87-1104, June 1987.

[23] Thomas, J. L., Taylor, S. K., and Anderson, W. K., "Navier-Stokes Computations of Vortical Flow over Low Aspect Ratio Wings," AIAA Paper 87-0207, Jan. 1987.

[24] Degani, C. and Schiff, L. B., "Computations of Supersonic Viscous Flows Around Pointed Bodies at Large Incidence," AIAA Paper 83-0034, Jan. 1983.

[25] Newsome, R. W. and Adams, M. S., "Numerical Simulations of Vortical-Flow over an Elliptical-Body Missile at High Angles of Attack," AIAA Paper 86-0559, Jan. 1986.

[26] Steger, J. L. and Sorenson, R. L., "Automatic Mesh Point Clustering Near Boundary in Grid Generation with Elliptic Partial Differential Equations," *Journal of Computational Physics*, Vol. 33, Dec. 1979, pp. 405–410.

[27] Sorenson, R. L., "A Computer Program to Generate Two-Dimensional Grids About Airfoils and Other Shapes by the Use of Poisson's Equation," NASA TM-81198, May 1980.

[28] Blottner, F. G., "Variable Grid Scheme Applied to Turbulent Boundary Layer," *Computer Methods in Applied Mechanics and Engineering*, Vol. 4, 1974, pp. 179–194.

[29] Kjelgaard, S. O., Sellers, W. L. III, and Weston, R. P., "The Flowfield over a 75 Degree Swept Delta Wing at 20.5 Degrees Angle of Attack," AIAA Paper 86-1775, June 1986.